Charge-carrier relaxation dynamics in highly ordered poly(*p*-phenylene vinylene): Effects of carrier bimolecular recombination and trapping

Cesare Soci, Daniel Moses,* Qing-Hua Xu,† and Alan J. Heeger
Center for Polymers and Organic Solids, University of California, Santa Barbara, California 93106-5090, USA
(Received 15 August 2005; revised manuscript received 19 October 2005; published 16 December 2005)

We have studied the charge-carrier relaxation dynamics in highly ordered poly(*p*-phenylene vinylene) over a broad time range using fast ($t>100$ ps) transient photoconductivity measurements. The carrier density was also monitored ($t>100$ fs) by means of photoinduced absorption probed at the infrared active vibrational modes. We find that promptly upon charge-carrier photogeneration, the initial polaron dynamics is governed by bimolecular recombination, while later in the subnanosecond time regime carrier trapping gives rise to an exponential decay of the photocurrent. The more sensitive transient photocurrent measurements indicate that in the low excitation regime, when the density of photocarriers is comparable to that of the trapping states ($\sim 10^{16}$ cm^{-3}), carrier hopping between traps along with transport via extended states determines the carrier relaxation, a mechanism that is manifested by a long-lived photocurrent "tail." This photocurrent tail is reduced by lowering the temperature and/or by increasing the excitation density. Based on these data, we develop a comprehensive kinetic model that takes into account the bipolar charge transport, the free-carrier bimolecular recombination, the carrier trapping, and the carrier recombination involving free and trapped carriers.

DOI: 10.1103/PhysRevB.72.245204 PACS number(s): 72.80.Le, 72.20.Jv, 73.50.Pz, 78.47.+p

I. INTRODUCTION

Unraveling the charge-carrier photogeneration, transport, and the carrier relaxation dynamics in conjugated polymers is of interest to gain fundamental understanding of this class of materials. Moreover, it is essential for designing efficient polymer-based devices such as light emitting diodes (LEDs), field effect transistors (FETs), and photovoltaic cells. A number of processes underlie the photocarrier transport in conjugated polymers, including carrier recombination, carrier trapping at localized states, carrier hopping between localized states, and transport via extended (band) states. In addition, the carrier mobility for the positive and negative polarons can vary with time as the carriers initially occupy extended states and later fall into progressively deeper trap states. The transport at any time regime is the result of the interplay between all the above operating processes.

Additionally, the mobility of the positive and negative carriers will in general be different. In the literature on polymer field effect transistors (FETs), there are many reports of unipolar *p*-type conduction.[1] However, it was recently shown that if the density of deep localized trapping states for electrons in the gate dielectric is reduced, *n*-channel FETs can be demonstrated with a large number of conjugated polymers.[2]

Typically, the high degree of disorder present in conjugated polymer films leads to high densities of traps, which mask the transport involving delocalized states. Thus in order to explore the intrinsic photoconduction mechanisms in these systems it is desirable to investigate samples with reduced trap density and/or to probe the transport at short times following excitation, before trap-limited mobility dominates the transport.

In this work we have implemented both approaches: we studied the carrier density and transport properties of a highly ordered sample of poly(*p*-phenylene vinylene) (PPV) with significantly improved structural order and reduced trap density by means of ultrafast ($t>100$ fs) time-resolved photoinduced absorption probed via the infrared active vibrational modes (IRAV) and fast ($t>100$ ps) transient photoconductivity measurements. The combination of these two techniques has allowed us to follow the carrier relaxation dynamics over more than five orders of magnitude in time after photoexcitation, and to separate the effects of traps from the intrinsic processes.

Our studies reveal the roles of bimolecular recombination and trapping on the photoconductive response. The data that comprise the transient photocurrent wave forms taken at various light intensities, electric fields, and temperatures are fitted to a kinetic model that includes bipolar charge transport, bimolecular recombination of free carriers, carrier trapping, and carrier recombination involving both trapped and free carriers. The model predicts the distinct time evolution of carrier occupation in localized trap states for both the positive and negative charges. The model also elucidates that the initial exponential decay of the photocurrent seen in many conjugated polymers in fact originates from the carrier trapping, behavior that has been attributed in earlier reports to the "monomolecular carrier recombination." We demonstrate that only a bimolecular carrier recombination term is required to obtain good understanding of both the IRAV and the transient photoconductivity data.

The paper is organized as follows: Section II describes the experimental details of our measurements. Section III presents results and discussions on the following issues: A. the concepts of bimolecular and monomolecular carrier recombination and their implication; B. the carrier dynamics probed by ultrafast IRAV photoinduced absorption measurements; C. the carrier transport and relaxation dynamics probed by fast transient photoconductivity measurements; D. the kinetic model we have developed to interpret the transient photoconductivity data. Section IV summarizes the findings and the conclusions derived from our study.

II. EXPERIMENTAL DETAILS

The PPV samples were free-standing films (with thickness between 14 and 17 μm), highly oriented by tensile drawing (with draw ratio of $l/l_0=4-5$). Their synthesis has been described elsewhere.[3,4] These oriented PPV films show a high degree of crystallinity and structural order.[5] As a result of the uniaxial alignment, the optical properties are highly anisotropic.[6,7] The alignment and structural order lead to enhanced charge photogeneration and charge transport properties.[8]

Ultrafast carrier density measurements were performed by means of photoinduced absorption of the IRAV modes in a standard pump and probe configuration. The pump beam ($\lambda_{pump}=400$ nm, beam diameter ~ 100 μm) utilized the second harmonic of a Ti:sapphire pulsed laser system (pulse duration of ~ 100 fs, repetition rate of 1 KHz). The probe beam ($\lambda_{probe}=9$ μm) was obtained by difference-frequency generation using the nonlinear crystal $AgGaS_2$.[9] Charge carriers on the polymer chains break the local translation symmetry and thereby convert Raman active modes into dipole-allowed infrared modes (IRAV),[10] a process that facilitates the optical probing of the photoinduced carrier density in conjugated polymers: thus, upon carrier photoexcitation or chemical doping, the IRAV signal is proportional to the charge-carrier density.[11,12] For the oriented PPV samples used in the present study, the IRAV signal at $\lambda_{probe}=9$ μm corresponds to the Raman mode observed around 1150 cm^{-1},[6,7] which was assigned to the C-C stretching and C-H bending of the phenyl ring.

Transient photoconductivity measurements were carried out in the Auston switch configuration[13] by mean of a boxcar integrating system, with an overall time resolution of about 100 ps. The PPV films were attached to an alumina (Al_2O_3) substrate, and planar Au contacts were evaporated on top of the film surface to form the photoconductive switch, with a gap between the electrodes between 10 and 20 μm. The contacts were deposited in such a way that the applied electric field was parallel to the polymer chain axis in the oriented film. In the surface electrode configuration, the applied electric field varies slightly across the polymer film thickness. We, however, have checked the magnitude of this effect by comparing the photoconductive response when illuminating the polymer films from the front and back sides (through a small hole in the alumina substrate) and found it to be negligible.

Figure 1 shows a schematic description of the photoconductive switch with the aligned PPV film on the alumina substrate; the polymer chain direction is indicated by the arrow. The pulsed laser beam illuminates the gap formed by the two Au electrodes deposited on the polymer film (from the left side). Figure 1 also depicts the profile of the transmitted light intensity (I_t/I_0) as a function of penetration depth (x), for linear excitation (at energy above the π-π^* transition) with polarization parallel ($L^{\parallel}$) and perpendicular ($L^{\perp}$) to the chain direction as well as the corresponding profile for two-photon (TP) excitation. These profiles were calculated using $I_t/I_0=e^{-\alpha x}$ for linear excitation and $I_t/I_0=(1+\beta I_0 x)^{-1}$ for two-photon excitation, where α is the linear absorption coefficient ($\alpha^{\parallel}=6\times10^5$ cm^{-1} and $\alpha^{\perp}=3\times10^4$ cm^{-1} at $\lambda=400$ nm),[6,7] and β is the two-photon absorption coefficient ($\beta^{\parallel}=68$ cm/GW at $\lambda=800$ nm).[14] Figure 1 indicates that low carrier densities can be achieved either by linear excitation with polarization perpendicular to the polymer chain axis, or alternatively via two-photon absorption,[15] as the longer optical penetration depth results in carrier photoexcitation across a greater volume. Due to the thickness of the polymer films (~ 15 μm), detectable photocurrent and IRAV signals could be achieved even for the lowest excitation densities used in our studies.[11,16] For the two-photon excitation, we used the output of a Ti:sapphire laser system ($\lambda=800$ nm), while for the one-photon excitation we utilized its second harmonic ($\lambda=400$ nm).

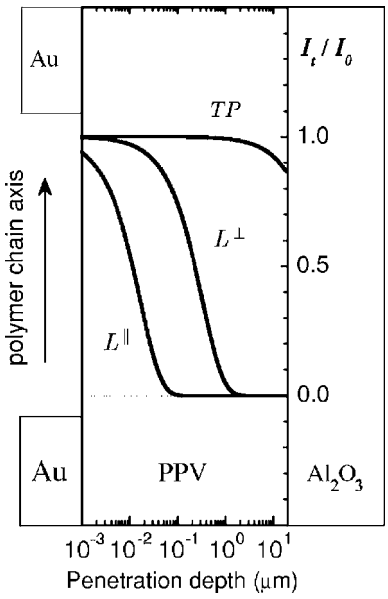

FIG. 1. Schematic diagram of the photoconductive switch that incorporates a thick, oriented PPV film. The light intensity profile as a function of the penetration depth (displayed on a logarithmic scale) is shown for linear excitation with polarization parallel ($L^{\parallel}$) and perpendicular ($L^{\perp}$) to the chain axis, as well as for two-photon (TP) excitation. The TP absorption was calculated for $I=120$ $\mu J/cm^2$, the lowest two-photon excitation intensity used in our experiments.

All measurements were performed while the samples were kept in vacuum (pressure of $<10^{-4}$ Torr). Low temperatures, down to 80 K, were obtained with a Helitran cryogenic system.

III. RESULTS AND DISCUSSION

A. Bimolecular vs monomolecular carrier recombination

Let us consider the case of a single kind of charge carrier (majority carrier) created by pulsed photoexcitation; in the absence of traps, photogenerated carriers can either undergo monomolecular recombination, according to the rate equation $dn/dt=-kn$, or bimolecular recombination, according to the rate equation $dn/dt=-\gamma n^2$, where $n(t)$ is the carrier density at a given time t, k is the monomolecular decay rate, and

γ is the bimolecular recombination coefficient. Therefore the decay of the population of charged species will be exponential $[n(t)=n_0\exp(-kt)]$ in the case of monomolecular recombination and algebraic $[n(t)=n_0/(n_0\gamma t+1)]$ in the case of bimolecular recombination, where $n_0=n(0)$ is the initial carrier density. Due to its linear dependence on excitation density, monomolecular recombination in conjugated polymers is often associated with geminate recombination of bound excitons, while bimolecular recombination can be indicative of free carrier recombination (polaron-polaron annihilation). It is straightforward to distinguish monomolecular and bimolecular recombination from the dependence of the carrier lifetime on excitation density: the monomolecular recombination is characterized by carrier lifetime independent of excitation density, while the bimolecular carrier recombination dynamics becomes faster as the excitation density increases. However, in the limit of $n_0\gamma t \gg 1$ the bimolecular decay becomes independent of excitation density, as indeed was observed in our IRAV experiments at excitation densities above $\sim 10^{20}$ cm^{-3} and/or at times greater than 10 ps.

B. Carrier density dynamics probed by ultrafast photoinduced IRAV

The oriented PPV films allowed us to perform IRAV measurements with probe polarized either parallel or perpendicular to the polymer chain axis. Probing with polarization parallel to the polymer chains leads to a tenfold IRAV signal, as compared to probing with perpendicular polarization, consistent with carrier delocalization along the polymer backbone. Figure 2 shows the intensity dependence of the IRAV signal, as obtained with pump polarized perpendicular and probe polarized parallel to the polymer chain axis. Previous photoinduced absorption experiments have demonstrated that charge-carrier photogeneration in conjugated polymers is an ultrafast process, and quantum efficiencies as high as 10–20 % have been deduced in high quality materials.[11,12,17] The ultrafast onset, promptly after excitation, of the IRAV signals in Fig. 2 confirms that charge-carrier photogeneration happens on a time scale faster than our experimental resolution ($\sim$300 fs). By taking into account the laser photon energy, intensity, laser beam size, the reflectivity, and the absorption coefficient of the sample, and assuming a carrier quantum yield of 10%,[12] we deduced the initial charge densities for the data in Fig. 2 to range from $n_0=1.5\times10^{19}$ to $n_0=1.3\times10^{20}$ cm^{-3}. Using these values for n_0, the IRAV dynamics for the different excitation densities have been fitted simultaneously to the bimolecular decay mechanism (solid curves in Fig. 2). Since at relatively high excitation densities the bimolecular carrier density decay approached a time scale comparable to the laser pulse duration, we have found it necessary to convolute the analytical expression with the laser temporal profile. From the optimization procedure, a bimolecular recombination coefficient of $\gamma=1.1\times10^{-8}$ $(\pm0.1\times10^{-8})$ cm^3/s was obtained, a typical value for large band-gap semiconductors[18] as well as for excitons and charge carriers in conjugated polymers.[19,20] Note that no satisfactory data fit could be achieved with a single exponential decay curve, which rules out a simple monomolecular dynamics. The inset of Fig. 2 shows the peak IRAV signal vs the excitation intensity. The linear behavior of the data (the solid line in the inset) rules out second-order processes for carrier photoexcitation (e.g., exciton-exciton annihilation). The latter is consistent with the direct carrier photogeneration mechanism inferred from the ultrafast onset of the IRAV signal.[11,12]

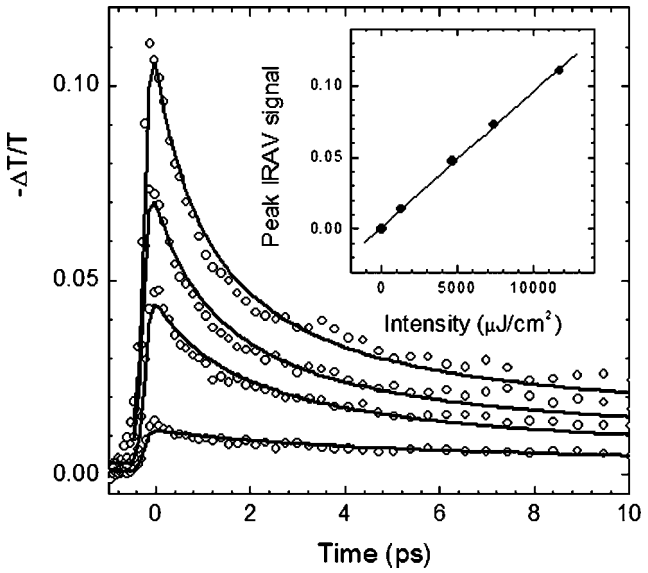

FIG. 2. Intensity dependence of the transient IRAV signal in oriented PPV, measured with perpendicular pump polarization and parallel probe polarization with respect to the polymer chain axis (open circles). From top to bottom, the displayed curves correspond to the following laser pulse intensities (initial carrier densities): 1.2×10^{-2} J/cm^2 $(1.3\times10^{20}$ cm$^{-3})$, 7.8×10^{-3} J/cm^2 $(8.5\times10^{19}$ cm$^{-3})$, 5×10^{-3} J/cm^2 $(5.4\times10^{19}$ cm$^{-3})$, and 1.4×10^{-3} J/cm^2 $(1.5\times10^{19}$ cm$^{-3})$. The solid lines are the fits to the data obtained for a bimolecular relaxation wave form, $n(t)=A+n_0/(1+n_0\gamma t)$, convoluted with the pulsed laser temporal profile (full width at half maximum of $\sim$300 fs). The inset shows the dependence of the peak IRAV signal on excitation intensity (dots); the solid line is a linear fit to the data.

IRAV measurements differ from photoconductivity measurements as they do not require an external electric field, and they are sensitive to both mobile and immobile (i.e., trapped) carriers. The persistent IRAV signal at long times might indeed result from the presence of trapped charges that survive the initial bimolecular annihilation and contribute to the photoinduced absorption signal.

C. Carrier transport and relaxation dynamics probed by transient photoconductivity

For a deeper understanding of the charge-carrier recombination dynamics in the presence of localized states, we have performed fast transient photocurrent (PC) measurements over a broad range of excitation intensities, temperatures, and applied electric fields. By taking advantage of the higher sensitivity provided by photoconductivity as compared to IRAV photoinduced absorption, we were able to utilize much lower excitation densities (up to a hundred times) compared

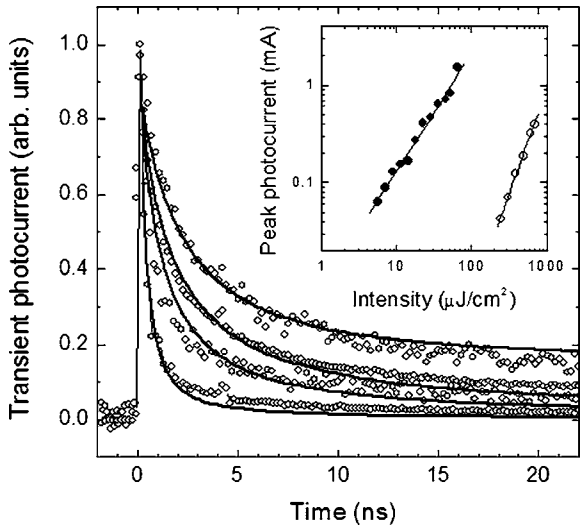

FIG. 3. Intensity dependence of the transient PC wave form obtained by one-photon excitation and light polarization perpendicular to the polymer chain axis (open circles); the displayed normalized curves, from top to bottom, were obtained for the following laser pulse intensities (initial carrier densities): 1×10^{-6} J/cm^2 (6.3×10^{15} cm^{-3}), 5.5×10^{-6} J/cm^2 (3.3×10^{16} cm^{-3}), 8.4×10^{-6} J/cm^2 (5.1×10^{16} cm^{-3}), 5.9×10^{-5} J/cm^2 (3.6×10^{17} cm^{-3}). The solid lines are obtained by Eqs. (1) with the optimal parameters reported in the text. The inset shows the dependence of the transient photocurrent peak on excitation intensity for linear excitation (solid dots) and two-photon excitation (open dots). The solid lines have linear coefficients $n=1.1$ and $n=2.1$, respectively.

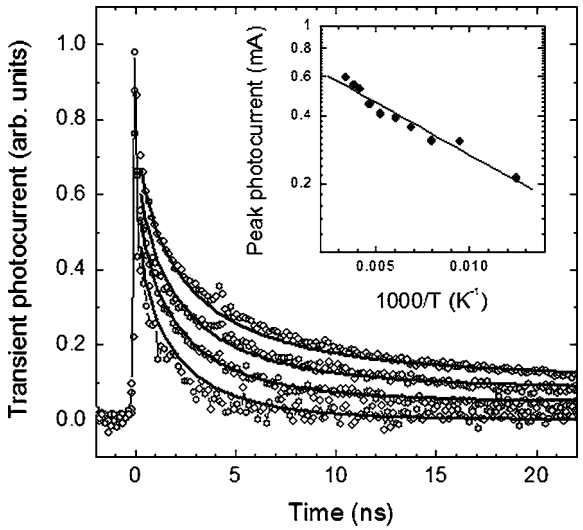

FIG. 4. Temperature dependence of the transient PC wave form generated by two-photon excitation (800 nm) at $F=3.3\times10^5$ V/cm and $I=1.2\times10^{-4}$ J/cm^2 per pulse (corresponding to an average initial carrier density of $\sim2\times10^{15}$ cm^{-3}). From top to bottom the curves are obtained at the following temperatures: 297, 290, 190, and 80 K. The solid curves are predicted by the kinetic model, with the parameters reported in the text. Inset: Arrhenius plot of the peak transient photocurrent (dots) and linear fit of the data (line), from which an activation energy of 45 meV is deduced.

to the smallest detectable IRAV signal, and to extend the observation time scale up to the microsecond regime, thus elucidating the slow relaxation mechanisms of charge carriers that survive the fast, initial recombination.

Figure 3 shows the normalized transient PC wave forms obtained via one-photon excitation with light polarized perpendicular to the polymer chain axis at various excitation intensities. For similar carrier densities, generated either by one- or two-photon absorption, we have detected similar PC wave forms (see Figs. 3 and 4), indicating that the carrier recombination dynamics is independent of the carrier generation route. A logarithmic plot of the intensity dependence of the peak transient PC for linear (perpendicular polarization) and two-photon excitation at various I is shown in the inset of Fig. 2. As expected, the data can be fitted by a power law with exponent $n\sim1$ and $n\sim2$ for one- and two-photon excitation, respectively. We note that the efficient charge-carrier photogeneration by two-photon absorption could be of interest for the realization of nonlinear photodetectors.[21] We have also verified that the contribution due to electron photoemission was negligible in these measurements (with both linear and nonlinear excitations) by checking the reproducibility of the experimental results while the sample chamber was filled with the electron quenching gas mixture CO_2+SF_6 (90%:10%).[22] Interestingly, we find the PC wave form independent of applied field F in the range of light intensities and electric fields ($F\leqslant3\times10^5$ V/cm) used in our measurements.

The PC wave form is found to be strongly dependent on excitation intensity; the higher is the intensity the faster is the PC decay rate, as indeed is expected from a bimolecular recombination process. From the carrier density onset of bimolecular recombination one can estimate the degree of delocalization of the polaron wave function: the lowest carrier density ($n\simeq2\times10^{15}$ cm^{-3}) used in our experiments sets a lower limit for the average intercarrier distance of $r=1/\sqrt[3]{n}\sim80$ nm, assuming isotropic probability for carrier recombination.

At low excitation intensities, the PC wave form exhibits a long-lived "tail" that persists out to the microsecond time regime, indicative of trap-mediated transport. The appearance of such a long-lived photocurrent reveals the effect of localized states that significantly extend the carrier lifetime via a trapping and de-trapping mechanism. Trap states can arise from structural (intrinsic) or chemical (extrinsic) defects such as grain boundaries between amorphous and crystalline regions or oxidation defects induced photochemically during the synthesis, or during the conversion of the precursor polymer.[23,24] Incorporated defects typically quench the photoluminescence and enhance the photoconductivity, thus playing a major role in the operation of organic devices. The density of trap states and their occupation in conjugated polymers have been the subject of extensive studies dealing with thermally stimulated currents (TSCs),[25–27] and space charge limited currents (SCLCs).[28] However, the study of localized states on the initial charge transport has been often overlooked.

Our interpretation of localized states as being responsible for the transition from free-carrier to trap-mediated transport

is corroborated by the temperature (T) dependence of the long-lived PC. As depicted in Fig. 4, as is T reduced, the PC tail diminishes. Below 100 K it is completely suppressed indicating that the carriers are "frozen" into the traps.[29] The effect of traps is manifested also at short time scales as indicated by the variation of the PC peak with T (Fig. 4, inset). The T dependence of the PC peak exhibits a weak thermally activated behavior that originates from the phonon assisted carrier release from traps operating during a time span comparable to the temporal resolution of our measuring system ($\sim$100 ps). The small activation energy (ΔE=45 meV) deduced from the temperature dependence of the PC indicates that shallow traps dominate the initial transport after photoexcitation.

D. Modeling the carrier dynamics in the presence of traps

Previous descriptions of slow carrier relaxation in conjugated polymers and glassy materials have often utilized a stretched-exponential (Kohlrausch) law,[30] which was interpreted either in terms of a distribution of carrier lifetimes[31–34] or in terms of time-dependent relaxation rates,[35–37] with the assumption that monomolecular (geminate) recombination was the only relevant photoconductive decay mechanism. Indeed, although bimolecular recombination has been frequently reported in studies of excitons and polarons dynamic probed by ultrafast photoinduced absorption,[19,38] so far the direct observation of bimolecular recombination in charge-transport measurements has been elusive, mainly due to the lack of sensitivity or time resolution and/or the availability of high quality conjugated polymers characterized by a small density of traps.

Carrier recombination hardly ever obeys solely bimolecular kinetics, due to competitive processes, such as charge localization in traps, a process that is manifested by an "apparent" monomolecular decay of the prompt photocurrent. In order to account for this latter mechanism, one should consider the rate equations for all the relevant impurity levels. Such a set of nonlinear differential equations turns out to be computationally very complicated and in general does not have an analytic solution.[39] Despite its complexity, this approach has been adopted successfully in a few studies of inorganic conventional semiconductors;[40–45] an approach we have adopted for analyzing the present data.

Our model accounts for the relevant rate equations, including carrier trapping and recombination at trap centers for both positively and negatively charged polarons, with the goal of deriving a unified, comprehensive description of the microscopic processes underlying the carrier transport and relaxation dynamics. The following scenario for the evolution of the charge transport has been considered: initially following pulsed photoexcitation, the generated charge carriers occupy extended states and promptly contribute to the transport. As time progresses, the "free" carrier density is reduced by (i) carriers annihilation via bimolecular (nongeminate) recombination, and (ii) localization of the carriers at trap sites. Carrier-phonon scattering may release the trapped carriers into extended states (detrapping process) and thus enable them to recontribute to the photocurrent. Once trapped, the carriers could also act as recombination centers; for example, a trapped negatively charged polaron could recombine with a mobile positively charged polaron. The polymer film contains several types of traps and/or recombination centers with distinct energy distributions for both electrons and holes. In order to limit the number of parameters, we assume that there is only one type of trap for electrons and one for holes, and whether they behave as traps or recombination centers is determined by a detrapping time parameter. The general description of the above processes can be formulated by the following set of differential equations:[46]

$$\begin{cases} \dfrac{d}{dt}n(t) = -\gamma n(t)p(t) - \beta_n[N_n - n_t(t)]n(t) + \dfrac{n_t(t)}{\tau_n} - \beta_{np_t}p_t(t)n(t), \\ \dfrac{d}{dt}n_t(t) = \beta_n[N_n - n_t(t)]n(t) - \dfrac{n_t(t)}{\tau_n} - \beta_{pn_t}n_t(t)p(t), \\ \dfrac{d}{dt}p(t) = -\gamma n(t)p(t) - \beta_p[N_p - p_t(t)]p(t) + \dfrac{p_t(t)}{\tau_p} - \beta_{pn_t}n_t(t)p(t), \\ \dfrac{d}{dt}p_t(t) = \beta_p[N_p - p_t(t)]p(t) - \dfrac{p_t(t)}{\tau_p} - \beta_{np_t}p_t(t)n(t), \end{cases} \tag{1}$$

where n and p indicate the density of mobile electrons and holes, n_t is the density of trapped electrons, p_t is the density of trapped holes, N_n is the density of trapping sites for electrons, and N_p is the density of trapping sites for holes; γ is the bimolecular recombination coefficient, β_n and β_p are the cross sections times the carrier velocity for free electron and hole trapping, β_{np} and β_{pn} are the cross sections times the carrier velocity for recombination of free electrons and holes with trapped holes and electrons; τ_n and τ_p are the electron and hole detrapping times. The carrier detrapping time is expected to exhibit a thermally activated behavior: $\tau = \nu^{-1}\exp(E_a/kT)$, where ν is the attempt-to-escape frequency and E_a is the activation energy for the detrapping process. A similar model has been recently employed for describing the

carrier recombination in the inorganic GaN.[18]

The photocurrent is given by

$$J_{PC}(t) = eF[\mu_n n(t) + \mu_p p(t)], \tag{2}$$

where e is the electron charge, F is the electric field, μ_n and μ_p are the electron and hole mobility in the extended states, and n and p are solutions of Eqs. (1) for the densities of electrons and holes, respectively. The theoretical electronic structure of PPV suggests that $\mu_n \approx \mu_p$,[47–49] a behavior that is consistent with the observation of the spatially resolved electroluminescence from oriented PPV in a planar metal-polymer-metal structure.[49] Equations (1) can be solved numerically and the optimal parameters obtained by minimizing the least squares deviation from the experimental data. For the nonlinear optimization we have used a program named EASY-FIT.[51]

We have used the following initial conditions: $n(0)=p(0)=n_0$ and $n_t(0)=p_t(0)=0$, where n_0 is again derived from the experimental excitation intensity, taking into account reflectivity, light penetration depth, and quantum yield for carrier photogeneration ($\phi=10\%$). The bimolecular recombination coefficient is given by $\gamma=1.1\times10^{-8}$ cm^3/s, as deduced from the IRAV experiment. We find that satisfactory fitting to the data can be achieved only if the detrapping time for one of the two types of charge carrier is much greater than 25 ns, indicating the presence of two types of traps, namely deep traps and shallow traps. Considering that pristine conjugated polymers typically show a p-type character,[27] we assume that electron traps are the deep ones, while hole traps are the shallow ones. With these assumptions all the remaining fitting parameters are uniquely determined by the optimization procedure.

From the simultaneous fitting of the entire set of intensity-dependent and temperature-dependent PC data (Figs. 3 and 4) we derived the following parameter values: total densities of traps of $N_n=0.6\times10^{16}$ ($\pm0.2\times10^{16}$) cm^{-3} and $N_p=4.6\times10^{16}$ ($\pm1.0\times10^{16}$) cm^{-3} (in agreement with the results of TSC (Ref. 52) and SCLC (Ref. 28) measurements carried on the highest quality materials), $\beta_n=8.1\times10^{-8}$ ($\pm3.2\times10^{-8}$) cm^3 s^{-1}, $\beta_p=23.1\times10^{-8}$ ($\pm12.2\times10^{-8}$) cm^3 s^{-1}, $\beta_{npt}=2.6\times10^{-8}$ ($\pm0.9\times10^{-8}$) cm^3 s^{-1}, $\beta_{pnt}=0.5\times10^{-8}$ ($\pm0.3\times10^{-8}$) cm^3 s^{-1}. The initial trapping times, for electrons and holes ($[\beta_{n,p}\times N_{n,p}]^{-1}$) are $\sim$2 ns and 100 ps, respectively. The deduced product of the cross section and the drift velocity for capturing free electrons is higher than that for free holes, consistent with the assumption of shallower hole traps. Note that although the electron traps are deeper than the hole traps, their lower density in conjunction with the significantly longer electron trapping time may result in trap-limited electron mobility comparable in magnitude to the hole mobility.[50]

Detrapping of holes from shallow traps extends the overall carrier lifetime. We find $\nu=1.28\times10^{11}$ ($\pm0.02\times10^{11}$) Hz and $E_a=67(\pm3)$ meV, which is comparable to the small activation energy of the measured transient PC peak (Fig. 4, inset). The energy of shallow traps is therefore $2-3k_BT$ (where T is room temperature). The corresponding hole detrapping time at room temperature is $\tau_p=8$ ps, while at 80 K it increases to $\tau_p=18$ ps. The carrier mobility can also be deduced from Eq. (2) once the time evolution of the carrier density is known (F is an experimental parameter). Assuming that the transport channel depth coincides with the light penetration depth, the current density is easily derived from the absolute values of the PC (inset of Fig. 2). This leads to an estimate for the carrier mobility for carriers in extended states of $\mu_n=\mu_p=1.6\times10^{-1}$ cm^2 V^{-1} s^{-1}, reflecting the high degree of structural order in the oriented PPV films.

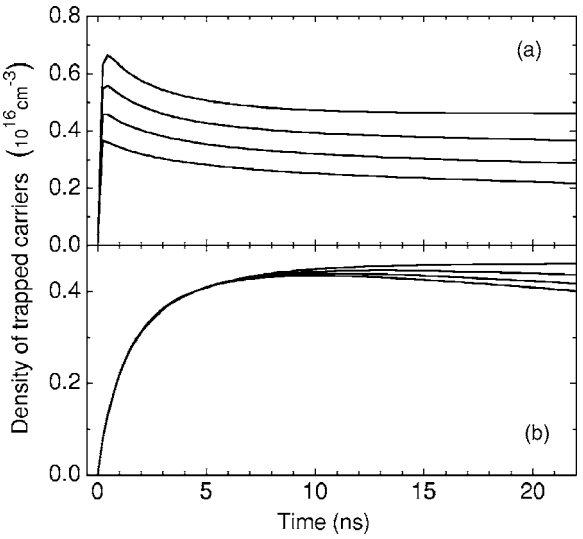

FIG. 5. Time evolution of the density of trapped holes (a) and trapped electrons (b) as predicted by the model for various temperatures; in both (a) and (b) the temperature corresponding to the different curves, from top to bottom, is 80, 190, 240, and 297 K.

Figure 5 shows the time evolution of the density of trapped electrons n_t (lower panel) and trapped holes p_t (upper panel), from solution of Eq. (1), for the optimal parameters we have determined. The assumption of relatively deep electron traps and shallow hole traps is manifested by the different behavior of electrons and holes after the initial fast thermalization. Independent of the temperature, electrons can barely escape from their traps within the time frame we have considered, while trapped holes are promptly released even at the lowest temperature considered (80 K); hole detrapping is more efficient at higher temperatures. The origin of traps responsible for imbalanced electron-hole transport in conjugated polymers has been the subject of recent theoretical studies (see Ref. 24 and references therein).

IV. CONCLUSIONS

In conclusion, we have studied the transient photoconductivity and carrier density in oriented and ordered PPV films at various excitation densities, temperatures, and external fields via impulse excitation ($\Delta t\sim100$ ps) using linear (400 nm) or two-photon (800 nm) absorption. The data indicate that the initial carrier dynamics is dominated by bimolecular recombination, even at the smallest light intensities utilized. The PC wave form is independent of the applied electric field (up to $F\sim3\times10^5$ V/cm) but strongly depen-

dent on excitation density and temperature. At high excitation densities, bimolecular recombination dominates the relaxation process, and thereby significantly reduces the photocarrier lifetime. From the lowest carrier density onset for bimolecular recombination we estimated a lower limit for the polaron delocalization of $r > 80$ nm. When the photogenerated carrier density is comparable to that of the trap states in the polymer film, the trap-limited dispersive transport is clearly evident from the long-lived photocurrent tail (up to 1 μs) that diminishes in relative magnitude at low temperatures.

The entire set of experimental results including the transient photocurrent wave forms taken at various light intensities, electric fields, and temperatures are fitted to a comprehensive kinetic model that accounts for bipolar charge transport, bimolecular recombination of free carriers, carrier trapping, and carrier recombination involving both trapped and free carriers. The model predicts the distinct time evolution of carrier occupation at localizing traps for both the positive and negative charges. The model also demonstrates that the initial exponential decay of the photocurrent seen in many conjugated polymers results from the apparent "monomolecular" process of carrier trapping. We demonstrate that only a bimolecular carrier recombination term is required in order to obtain a good fit to the data. Fitting the transient PC wave forms to the kinetic model also provides total density of traps of $\sim 10^{16}$ cm^{-3} and carrier mobility of $\mu_n = \mu_p = 1.6 \times 10^{-1}$ cm^2 V^{-1} s^{-1}, indicative of the structural order of the PPV films.

The long-lived photocurrent indicates the importance of structural order in the PPV films; as a result of the material quality, there is a relatively small density of shallow traps. Although these traps reduce the "effective" carrier mobility, they significantly extend the carrier lifetime, up to $t > 1$ μs. This observation indicates that for some device applications the reduced carrier mobility can be compensated adequately by the longer carrier lifetime. In particular this is applicable in devices such as photovoltaic cells in which the carrier collection efficiency (and thus the device power efficiency) depends on the recombination length that is proportional to the product of the carrier mobility and carrier lifetime ($\mu\tau$).

ACKNOWLEDGMENTS

We thank Professor Paulo Miranda for providing us with some preliminary IRAV data and Dr. Raluca Negres and Dr. In-Wook Hwang for useful discussions. This work was supported by the National Science Foundation under contract Nos. DMR-0099843 and DMR-0096820.

*Author to whom correspondence should be addressed. Email address: moses@ipos.ucsb.edu

†Present address: Department of Chemistry, National University of Singapore, 3 Science Drive 3, Singapore 117543.

[1] C. D. Dimitrakopoulos and P. R. L. Malenfant, Adv. Mater. (Weinheim, Ger.) **14**, 99 (2002).

[2] L. L. Chua, J. Zaumseil, J. F. Chang, E. C. W. Ou, P. K. H. Ho, H. Sirringhaus, and R. H. Friend, Nature (London) **434**, 194 (2005).

[3] T. Ohnishi, T. Noguchi, T. Nakano, M. Hirooka, and I. Murase, Synth. Met. **41**, 309 (1991).

[4] S. Kuroda, T. Noguchi, and T. Ohnishi, Phys. Rev. Lett. **72**, 286 (1994).

[5] C. Y. Yang, K. Lee, and A. J. Heeger, J. Mol. Struct. **521**, 315 (2000).

[6] C. Soci, D. Comoretto, F. Marabelli, and D. Moses, Proc. SPIE **5517**, 98 (2004).

[7] D. Comoretto, G. Dellepiane, F. Marabelli, J. Cornil, D. A. dos Santos, J. L. Bredas, and D. Moses, Phys. Rev. B **62**, 10173 (2000).

[8] C. H. Lee, J. Y. Park, Y. W. Park, D. Moses, A. J. Heeger, T. Noguchi, and T. Ohnishi, Synth. Met. **101**, 444 (1999).

[9] M. K. Reed and M. K. Steiner-Shepard, *Ultrafast Phenomena X: Proceedings of the 10th International Conference, del Coronado, CA, 1996* (Springer, Berlin, New York, 1996).

[10] B. Horovitz, Solid State Commun. **41**, 729 (1982).

[11] D. Moses, A. Dogariu, and A. J. Heeger, Phys. Rev. B **61**, 9373 (2000).

[12] P. B. Miranda, D. Moses, and A. J. Heeger, Phys. Rev. B **64**, 081201 (2001).

[13] D. H. Auston, IEEE J. Quantum Electron. **19**, 639 (1983).

[14] R. A. Negres (unpublished).

[15] M. Samoc, A. Samoc, and B. Luther-Davies, Synth. Met. **109**, 79 (2000).

[16] C. Soci and D. Moses, Synth. Met. **139**, 815 (2003).

[17] A. Ruseckas, M. Theander, M. R. Andersson, M. Svensson, M. Prato, O. Inganas, and V. Sundstrom, Chem. Phys. Lett. **322**, 136 (2000).

[18] F. Binet, J. Y. Duboz, E. Rosencher, F. Scholz, and V. Harle, Appl. Phys. Lett. **69**, 1202 (1996).

[19] A. Dogariu, D. Vacar, and A. J. Heeger, Phys. Rev. B **58**, 10218 (1998).

[20] G. Dicker, M. P. d. Haas, L. D. A. Siebbeles, and J. M. Warman, Phys. Rev. B **70**, 045203 (2004).

[21] M. Samoc, A. Samoc, B. LutherDavies, A. Dowd, and M. McDonnell, J. Phys. D **30**, 895 (1997).

[22] D. Moses, C. Soci, P. Miranda, and A. J. Heeger, Chem. Phys. Lett. **350**, 531 (2001).

[23] F. Papadimitrakopoulos, K. Konstadinidis, T. M. Miller, R. Opila, E. A. Chandross, and M. E. Galvin, Chem. Mater. **6**, 1563 (1994).

[24] H. F. Meng and Y. S. Chen, Phys. Rev. B **70**, 115208 (2004).

[25] A. A. Alagiriswamy and K. S. Narayan, J. Appl. Phys. **91**, 3021 (2002).

[26] M. Meier, S. Karg, K. Zuleeg, W. Brutting, and M. Schwoerer, J. Appl. Phys. **84**, 87 (1998).

[27] V. Kazukauskas, Semicond. Sci. Technol. **19**, 1373 (2004).

[28] Z. Chiguvare and V. Dyakonov, Phys. Rev. B **70**, 235207 (2004).

[29] D. Moses, M. Sinclair, and A. J. Heeger, Phys. Rev. Lett. **58**, 2710 (1987).

[30] G. Dicker, M. P. de Haas, D. M. de Leeuw, and L. D. A. Siebbeles, Chem. Phys. Lett. **402**, 370 (2005).
[31] H. Scher and E. W. Montroll, Phys. Rev. B **12**, 2455 (1975).
[32] H. Scher, M. F. Shlesinger, and J. T. Bendler, Phys. Today **44** (1), 26 (1991).
[33] M. F. Shlesinger and E. W. Montroll, Proc. Natl. Acad. Sci. U.S.A. **81**, 1280 (1984).
[34] H. Bassler, Phys. Status Solidi B **175**, 15 (1993).
[35] J. Kakalios, R. A. Street, and W. B. Jackson, Phys. Rev. Lett. **59**, 1037 (1987).
[36] B. Dulieu, J. Wery, S. Lefrant, and J. Bullot, Phys. Rev. B **57**, 9118 (1998).
[37] C. H. Lee, G. Yu, and A. J. Heeger, Phys. Rev. B **47**, 15543 (1993).
[38] E. Maniloff, V. Klimov, and D. W. McBranch, Phys. Rev. B **56**, 1876 (1997).
[39] R. H. Bube, *Photoconductivity of Solids* (R.E. Krieger, Huntington, NY, 1978).
[40] A. Rose, *Concepts in Photoconductivity and Allied Problems* (Interscience, New York, 1963).
[41] S. M. Ryvkin, *Photoelectric Effects in Semiconductors* (Consultants Bureau, New York, 1964).
[42] N. V. Joshi, *Photoconductivity: Art, Science, and Technology* (M. Dekker, New York, 1990).
[43] N. V. Joshi, Phys. Rev. B **27**, 6272 (1983).
[44] N. V. Joshi, Phys. Rev. B **32**, 1009 (1985).
[45] R. Chen, S. W. S. McKeever, and S. A. Durrani, Phys. Rev. B **24**, 4931 (1981).
[46] S. Wang, *Solid-state Electronics* (McGraw-Hill, New York, 1966).
[47] P. Gomes Dacosta and E. M. Conwell, Phys. Rev. B **48**, 1993 (1993).
[48] N. Kirova, S. Brazovskii, and A. R. Bishop, Synth. Met. **100**, 29 (1999).
[49] J. L. Bredas, B. Themans, J. G. Fripiat, J. M. Andre, and R. R. Chance, Phys. Rev. B **29**, 6761 (1984).
[50] U. Lemmer, D. Vacar, D. Moses, A. J. Heeger, T. Ohnishi, and T. Noguchi, Appl. Phys. Lett. **68**, 3007 (1996).
[51] K. Schittkowski, *Numerical Data Fitting in Dynamical Systems: A Practical Introduction with Applications and Software* (Kluwer Academic, Dordrecht, Boston, 2002).
[52] E. J. W. List, C. H. Kim, J. Shinar, A. Pogantsch, G. Leising, and W. Graupner, Appl. Phys. Lett. **76**, 2083 (2000).